Topography of inland deltas: Observations, modeling, and experiments

H. J. Seybold,[1] P. Molnar,[2] D. Akca,[3] M. Doumi,[1,4] M. Cavalcanti Tavares,[5] T. Shinbrot,[4] J. S. Andrade Jr.,[5] W. Kinzelbach,[2] and H. J. Herrmann[1,5]

Received 10 December 2009; revised 26 January 2010; accepted 29 January 2010; published 28 April 2010.

[1] The topography of inland deltas is influenced by the water-sediment balance in distributary channels and local evaporation and seepage rates. In this letter a reduced complexity model is applied to simulate inland delta formation, and results are compared with the Okavango Delta, Botswana and with a laboratory experiment. We show that water loss in inland deltas produces fundamentally different dynamics of water and sediment transport than coastal deltas, especially deposition associated with expansion-contraction dynamics at the channel head. These dynamics lead to a systematic decrease in the mean topographic slope of the inland delta with distance from the apex following a power law with exponent $\alpha = -0.69 \pm 0.02$ where the data for both simulation and experiment can be collapsed onto a single curve. In coastal deltas, on the contrary, the slope increases toward the end of the deposition zone. **Citation:** Seybold, H. J., P. Molnar, D. Akca, M. Doumi, M. Cavalcanti Tavares, T. Shinbrot, J. S. Andrade Jr., W. Kinzelbach, and H. J. Herrmann (2010), Topography of inland deltas: Observations, modeling, and experiments, *Geophys. Res. Lett.*, *37*, L08402, doi:10.1029/2009GL041605.

1. Introduction

[2] Inland deltas can be found in several places around the world, e.g. in Botswana (Okavango), the Sudan (The Sudd) or Slovakia (Danube). Although the plan view of diverging channel networks look quite similar, inland deltas and coastal deltas are morphologically very distinct.

[3] Their deposition patterns are influenced by different dominant fluvial processes and boundary conditions. Coastal deltas are dominated by wave/tide actions and coastal currents separating the subaerial and subaqueous parts [*Fagherazzi*, 2008]. Inland deltas, on the other hand, are dominated by channel flow influenced by evapotranspiration, infiltration, and the growth of bank and island-stabilizing vegetation. Because of these additional complex processes and feedbacks, inland deltas are less well studied than their coastal counterparts.

[1]Computational Physics for Engineering Materials, ETH Zurich, Zurich, Switzerland.
[2]Institute of Environmental Engineering, ETH Zurich, Zurich, Switzerland.
[3]Department of Information Technologies, Isik University, Istanbul, Turkey.
[4]Department of Biomedical Engineering, Rutgers University, Piscataway, New Jersey, USA.
[5]Departamento de Geologia, Universidade Federal do Ceará, Ceará, Brazil.

0094-8276/10/2009GL041605

[4] In this letter we investigate the geomorphological features of inland deltas, and compare them with coastal ones. In particular we analyze the general topographic signature of the Okavango Delta, which is one of the largest inland deltas. The results are also compared with a new reduced complexity model [*Seybold et al.*, 2007] and with a small-scale laboratory experiment.

[5] The model applied in this case reduces the complexity of the hydrological and sedimentary equations while maintaining the essential physics. The first version of the model reported by *Seybold et al.* [2007] simulates coastal delta formation successfully. Here the model is extended to include water loss to study the morphogenesis of inland deltas.

[6] To investigate the processes leading to the rich inland delta morphology, we accompany the computational model with a laboratory-scale flume experiment. Flume experiments on delta formation have been carried out in the last years in several laboratories [*Hoyal and Sheets*, 2009; *Martin et al.*, 2009]. Also recently, the formation of alluvial fans caused by rapid water release has been studied by *Kraal et al.* [2008]. However, experimental work on inland deltas including evaporation is new. We use these experiments as a verification for the modeling and as a tool to understand the interplay between the dominant sedimentation processes.

2. Computational Modeling

[7] For the simulation of inland delta formation, we have extended the model of *Seybold et al.* [2007, 2009]. The water loss through evapotranspiration is included in the conservation equations of the water flow by adding a sink term E_i in each node. The water level above the ground is updated as follows:

$$V_i = V_i' + \delta t \sum_{N.N.} (I_{ij} + E_i), \tag{1}$$

where the sum runs over the four nearest neighbors (*N.N.*) of a given node. The variable V_i indicates the new water surface on node i and V_i' is the water level of the previous step. I_{ij} is the flow between nodes i and j. E_i defines the loss of water due to evaporation or infiltration in node i. The loss rate is modeled by a phenomenological formula $E_i = d_i \cdot \hat{E}$ where $\hat{E}$ defines the maximum loss rate. The increase of seepage in the distal parts of the delta is modeled by the variable d_i which is the normalized distance of the cell from the inlet.

[8] As initial condition we use an inclined plane distorted by random perturbations. Open boundary conditions are applied on all sides except in the inlet nodes where water is injected into the domain. In order to describe inland delta

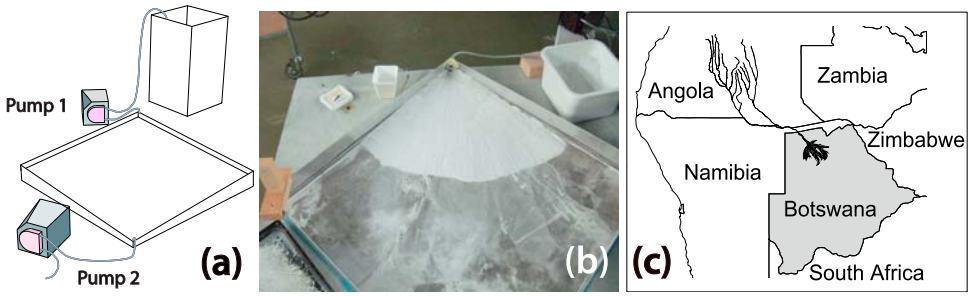

Figure 1. Sketch of the experimental setup. (a) Water and sediment are fed from a container. The sediment is kept in suspension using an electric mixer and then is injected into the basin using a peristaltic pump (Ismatec ecoline, pump 1). Remaining water is pumped out of the basin (pump 2). (b) Initial condition of the experiment. (c) Map of the location of the Okavango Delta [*Milzow et al.*, 2009].

development processes, two types of channel ends need to be included: newly forming channels where $dI = I(t + \delta t) - I(t) > 0$ do not show sedimentation at the front, and channels that are drying $dI < 0$ show high deposition rates at their terminal ends where deposition is applied according to equation (4) of *Seybold et al.* [2009].

[9] In the model, the processes of evaporation and infiltration lead to complex dynamics: channel extension takes place due to erosion and contraction due to deposition at the channel heads, which is not present in wet deltas. Furthermore, the model reproduces the development of bank levees by lateral deposition on channel margins. The natural formation of bank levees by overbank deposition occurs in the Okavango and in many natural dryland rivers [*McCarthy et al.*, 1988] due to riparian vegetation and other processes that are notoriously difficult to simulate. Furthermore, riparian vegetation affects not only deposition but also evapotranspiration and infiltration rates. These effects need to be included in future inland delta models.

3. Experimental Modeling

[10] Our setup consists of a 1 × 1 m aluminum basin, fixed at an inclination of about 6 degrees running along the basin diagonal. An initial surface is created using a uniformly sloped sediment layer with an height of 5 cm at the inlet (Figure 1).

[11] We use crushed glass as sediment with diameter 50 to 120 microns and a bulk density of $\varrho = 2.2$ g/cm^3. The sediment is continuously mixed with water using a marine-type impeller in an upstream tank. This mixture is injected at a steady rate into the basin using a peristaltic pump. The volumetric sediment concentration is approximately 0.05 and the inflow is set to 1000 ml/h. To simulate the boundary conditions of the dry delta, infiltrated water which accumulates at the bottom edge is continuously pumped out. In addition water is evaporated by an array of fifteen 300W heat lamps that are fixed 15 cm above the surface.

[12] The experiment is run as follows: a water/sediment mixture is injected into the flume over 45 minutes, followed by drying over 2:15 hours. We call one period of injection and drying an "epoch", where epoch 0 denotes the initial condition (Figure 1b). After complete drying, the surface topography is scanned using a Breukmann OptoTOP-SE 3D scanner. The scanning technique is based on a stereoscopic measurement, in which regular fringes are projected onto the surface and the stripes' deformations are measured using a CCD camera. From the deformations of these lines the topography can be reconstructed with an accuracy of 100 microns [*Burke et al.*, 2002; *Akca et al.*, 2007]. Several scans have to be combined into a co-registered mosaic to cover the entire surface, using a least square matching method [*Gruen and Akca*, 2005]. An invariant reference point outside of the sedimentation domain is used to co-register the different sediment layers. Thus we obtain temporal and spatial distributions of sediment during the experiment. For the wet delta experiment we remove the heat lamps and change the boundary conditions at the downstream end of the flume to preserve a constant water level, while keeping the other parameters unchanged.

4. Analysis of Inland Delta Formation

[13] Visually, the computational inland delta model produced deposition structures and channels similar to natural deltas. We quantify these similarities by estimating the fractal dimension of simulated and observed delta networks with the box counting method [*Feder*, 1989; *Turcotte*, 1997]. A least squares fit of a power law $N \sim s^{-D}$, to the data yields a fractal dimension $D = 1.85 \pm 0.05$ for the Okavango Delta, as compared with the simulation result of $D = 1.84 \pm 0.05$. The pattern of the flooded area of the Okavango is extracted through the vegetation cover by a combined analysis of high resolution aerial photos from GoogleEarth™ and NOAA satellite measurements.

[14] These numbers are quite close to those derived for coastal deltas [*Seybold et al.*, 2007]. Together with a similar diverging channel structure this leads impression that both systems are formed by the similar processes. In the following we show by analyzing the topography that the two systems show completely distinct morphological structures.

[15] A useful topographic metric to quantify the shape of a delta is the mean slope as a function of downstream distance from the delta apex. We define the mean topographic slope $S(d)$ averaged over circular arcs at a distance $[d, d + dr]$ from the delta apex. In order to compare the different observed, numerical and experimentally modeled deltas, we normalize the surface slopes with the overall spatial mean,

$$S(d) = \frac{1}{\langle S \rangle} \langle S \rangle_{d+dr}. \quad (2)$$

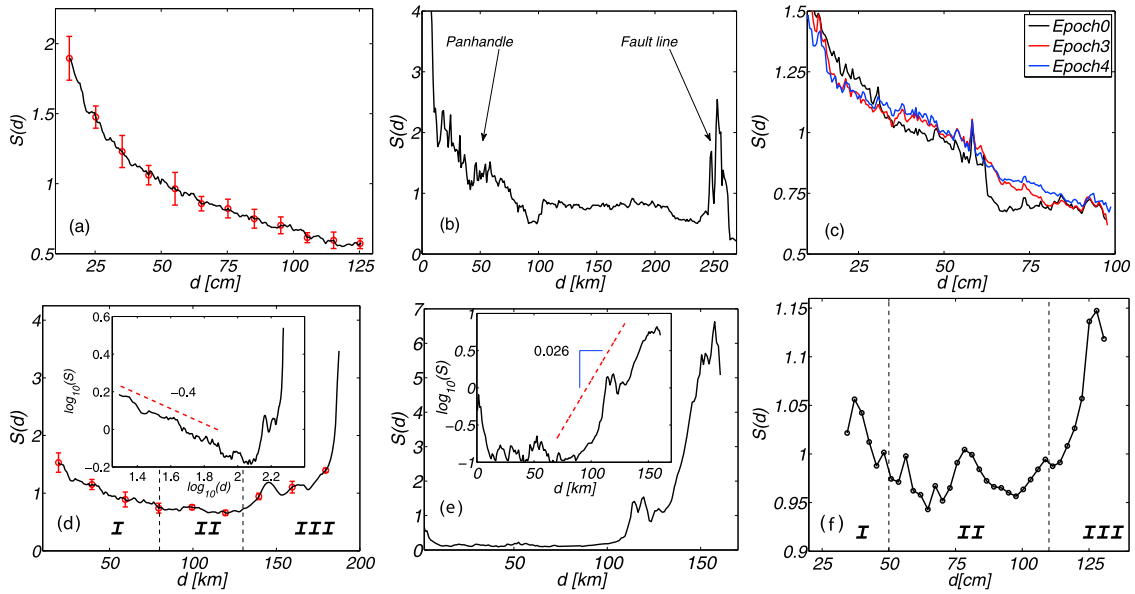

Figure 2. Plot of the slope $S(d)$ (a) for the simulation averaged over 9 samples, the errorbars indicate the statistical error, (b) the Okavango derived from DEM data, and (c) the experiment (initial condition, epochs 3 and 4). Both experiment and simulation show a similar decreasing slope with distance from the apex. Figures 2d–2f show the slope $S(d)$ from equation (2) for wet deltas: (d) Simulation, (e) the Mississippi, and (f) the wet experiment. The average slope for wet deltas is different from that of dry deltas in Figures 2a–2c. Simulation and experiment show an initial part with deceasing slope (I) where the stream adjusts the inclination to its transport capacity followed by a part of almost constant slope (II) and a strongly increasing part at the delta end (III). The inset of the simulation in Figure 2d shows that the initial slope decreases like a power law with exponent $\alpha = -0.4 \pm 0.03$.

The averages are computed on circular arcs over a spatial domain which contains the whole delta surface. $S(d)$ is a useful topographic measure of the fluvial system including the boundary conditions for two reasons.

[16] First, it is an integral measure of the processes of deposition in space at an equal distance from the apex. Second, topographic slope is a fundamental variable for sediment transport in transport capacity-limited conditions such as inland delta distributary channels. For coastal deltas the average floodplain (including channel bottoms) gives a measure between the channel slope and the energy slope. Other statistical measures for coastal deltas have been proposed by *Jerolmack and Swenson* [2007].

[17] In order to compare Okavango, experiment, and simulated topography more directly, we have rescaled the horizontal extents of the simulation to fit the experimental domain. A comparison of $S(d)$ for the modeled surface, the experiment and the Okavango DEM surface [*Gumbricht et al.*, 2005] is shown in Figure 2.

[18] The modeled surface gradually decreases in $S(d)$ downstream as the sediment transport capacity in smaller (but more numerous) channels is reduced due to evaporation and seepage of water. The delta becomes flatter as a consequence. Concavity in the surface profile along the delta is expected. This has been demonstrated both in fluvially-formed landscapes [e.g., *Sinha and Parker*, 1996] and in the shape of submarine canyons [e.g., *Gerber et al.*, 2009] under equilibrium steady-state conditions. Concavity in the surface profile is the result of the physically-based formulation of water and sediment fluxes in the model.

[19] Local variations may be associated with the varying heads of individual distributary channels which may be actively eroding and so can be expected to have a higher local slope. Figure 2a displays the simulated slope averaged over nine simulation runs with the same evaporation rate and boundary conditions, but different random perturbations (approx. 1%) to the initial surface. The parameters for this simulation have been chosen to be $I_0 = 1 \times 10^{-3}$ (water inflow), $I^* = -7.5 \times 10^{-6}$ (erosion threshold), $s_0 = 0.0025$ (sediment inflow), $c = 0.1$ (erosion strength from *Seybold et al.* [2009]). The evaporation rate in this case is set to $\hat{E} = 5 \times 10^{-8}$. As shown in the inset of Figure 3, the local slopes obtained from the dry delta experiments as well as from model simulations follow power-law behavior, $S = a(d - d_0)^{\alpha}$. The least-squares fit to the data indicates that both a and d_0 depend on particular conditions, like the starting point d_0 of the measurement. More striking is the fact that we obtain identical power-law exponents $\alpha = -0.69 \pm 0.02$ for experimental data and model simulations after rescaling S to $S^* = S/a$ and plotting it against $d^* = d - d_0$.

[20] In reality, the Okavango surface shows a more complex behavior affected strongly by local geology and tectonics (Figure 2b). During the first 100 km the Okavango is confined between fault lines forming a confined area called the Panhandle. Outside the Panhandle the delta surface is almost totally flat with only small local variability around the constant slope of the fan. The increase in mean slope at the bottom end of the delta is a consequence of the Kunyere and Thamalakane fault lines [see, e.g., *Milzow et al.*, 2009].

[21] The downstream distribution of slope also highlights the fundamental difference between wet (coastal) and dry

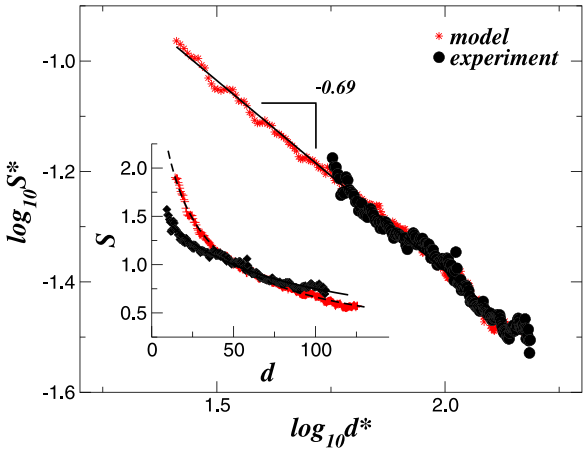

Figure 3. Scaling of the rescaled slope S^* with rescaled distance d^* of the form $S^* \sim (d^*)^{\alpha}$ with $\alpha = -0.69 \pm 0.02$ for the simulations (red stars) and experiment (black circles). The inset shows the decay of the slope for experiment (epoch 5, black diamonds) and model (red crosses) together with the corresponding least-square fits of a power-law to the data for the unscaled variables S and d.

(inland) deltas. The Mississippi Delta Balize Lobe profile from bathymetric data *Divins and Metzger* [2006] shows that in coastal deltas the mean slope increases downstream as the distributary channels enter the ocean and sediment deposition becomes limited by the settling velocity of particles and their advection by currents and tides (Figure 2e). This leads to a terminal point where most of the coarse sediment is deposited corresponding to the transition from channel flow to coastal current. In the DEM and bathymetric data of the Balize Lobe the slope then increases exponentially at the (pro)delta front (Figure 2e).

[22] Furthermore with time the Mississippi River has adjusted the average slope to the optimal transport capacity of the stream resulting in a constant slope on the coastal plain.

[23] A strongly increasing slope toward the end of the lobes is also observed in the simulations of *Seybold et al.* [2009] shown in (Figure 2d), averaged over 5 different runs with the same set of parameters but different initial random surface noise. The parameters are identical to those of *Seybold et al.* [2009]. We observe from the simulation that the river first adjusts the slope imposed by the initial conditions to its transport capacity (Figure 2d, part I) until it flows at an almost constant slope in the newly formed lobe (Figure 2d, part II, between d = 80–120 km). The decay of the slope in the initial part I fits a power law with exponent around $\alpha \approx -0.4$.

[24] The same phenomenon is observed in the wet delta experiment (Figure 2f), i.e., a decreasing slope in the initial part of the delta where the stream adjusts the base slope due to erosion and deposition (Figure 2f, part I), constant slope in the central part where sediment is transferred (Figure 2f, part II), and an increase in slope toward the delta front (Figure 2f, part III).

5. Conclusions

[25] In this paper we have applied a reduced complexity model which was originally developed for coastal deltas [*Seybold et al.*, 2009] to an inland delta, using the Okavango as reference. Elevation and slope based metrics have been used to describe the delta shape and change. Furthermore we have set up a small-scale laboratory experiment to verify the modeling results and elucidate the time evolution of the delta system. In inland deltas the sediment load from upstream is distributed along the active channels in a more spatially distributed manner than in coastal deltas where deposition occurs mostly on the coastal interface and leads to gradual delta progradation. These differences in the boundary conditions induced by the evaporation and seepage concerning inland deltas and the standing water level in the case of coastal deltas lead to a fundamentally different morphology.

[26] In particular, the expansion-contraction dynamics at the channel heads and the consequent deposition lead to a consistent decrease in mean topographic slope with distant to the apex in the cae of inland deltas. The decrease of the slope in the experiment as well as in the simulation shows a clear power law behavior. By rescaling variables we have collapsed the two curves on a single power law with exponent $\alpha = -0.69 \pm 0.02$.

[27] The simple topographic measure presented, highlights the difference between inland and coastal deltas insofar as topographic slope in the latter case increases dramatically at the land-ocean interface. For the further investigation of the delta formation process it is planed to relate the topographic features and surface characteristics with the hydrological variables of the fluvial system.

[28] **Acknowledgments.** This work was funded by the Swiss National Foundation grant NF20021-116050/1. The author D.A. was affiliated to the Institute of Geodesy and Photogrammetry of ETH Zurich when performing the project. J.S.A.J would like to thank the Brazilian agencies CNPq, CAPES and FUNCAP for financial support.

References

Akca, D., F. Remondino, D. Novàk, T. Hanusch, G. Schrotter, and A. Gruen (2007), Performance evaluation of a coded structured light system for cultural heritage applications, in *Videometrics IX*, *Proc. SPIE*, *6491*, 64910V (2007), doi:10.1117/12.705578.

Burke, J., T. Bothe, W. Osten, and C. Hess (2002), Reverse engineering by fringe projection, in *Interferometry XI: Applications*, *Proc. SPIE*, *4778*, 312–324.

Divins, D., and D. Metzger, (2006), NGDC Coastal Relief Model, Natl. Geophys. Data Cent., Boulder, Colo. (Available at http://www.ngdc.noaa.gov/mgg/coastal/coastal.html)

Fagherazzi, S. (2008), Self-organization of tidal deltas, *Proc. Natl. Acad. Sci. U. S. A.*, *105*(48), 18,692–18,695, doi:10.1073/pnas.0806668105.

Feder, J. (1989), *Fractals*, 4 ed., Plenum, New York.

Gerber, T., D. Amblas, M. Wolinski, L. Pratson, and M. Canals (2009), A model for the long-profile shape of submarine canyons, *J. Geophys. Res.*, *114*, F03002, doi:10.1029/2008JF001190.

Gruen, A., and D. Akca (2005), Least squares 3d surface and curve matching, *J. Photogramm. Remote Sens.*, *59*(3), 151–174.

Gumbricht, T., T. S. McCarthy, and P. Bauer (2005), Micro-topography of the Okavango Delta wetlands, *Earth Surf. Processes Landforms*, *30*, 27–29, doi:10.1002/esp.1124.

Hoyal, D., and B. Sheets (2009), Morphodynamic evolution of cohesive experimental deltas, *J. Geophys. Res.*, *114*, F02009, doi:10.1029/2007JF000882.

Jerolmack, D. J., and J. B. Swenson (2007), Scaling relationships and evolution of distributary networks on wave-influenced deltas, *Geophys. Res. Lett.*, *34*, L23402, doi:10.1029/2007GL031823.

Kraal, E., M. van Dijk, G. Postma, and M. Kleinhans (2008), Martian stepped-delta formation by rapid water release, *Nature*, *451*, 973–976, doi:10.1038/nature06615.

Martin, J., B. Sheets, C. Paola, and D. Hoyal (2009), Influence of steady base-level rise on channel mobility, shoreline migration, and scaling

properties of cohesive experimental delta, *J. Geophys. Res.*, *114*, F03017, doi:10.1029/2008JF001142.

McCarthy, T. S., K. H. Rogers, I. G. Stanistreet, W. N. Ellery, B. Cairncross, K. Ellery, and T. Gorbicki (1988), Features of channel margins in the Okavango Delta, *Palaeoecol. Africa*, *19*, 3–14.

Milzow, C., L. Kgotlhang, P. Bauer-Gottwein, P. Meier, and W. Kinzelbach (2009), Regional review: the hydrology of the okavango delta, Botswana, processes, data and modelling, *Hydrol. J.*, *17*, 1297–1328, doi:10.1007/s10040-009-0436-0.

Seybold, H. J., J. S. Andrade Jr., and H. J. Herrmann (2007), Modeling river delta formation, *Proc. Natl. Acad. Sci. U. S. A.*, *104*(43), 16,804–16,809, doi:10.1073/pnas.0705265104.

Seybold, H. J., P. Molnar, H. M. Singer, J. S. Andrade Jr., H. J. Herrmann, and W. Kinzelbach (2009), Simulation of birdfoot delta formation with application to the Mississippi Delta, *J. Geophys. Res.*, *114*, F03012, doi:10.1029/2009JF001248.

Sinha, S. K., and G. Parker (1996), Causes of concavity in longitudinal profiles of rivers, *Water Resour. Res.*, *32*, 1417–1428, doi:10.1029/95WR03819.

Turcotte, D. (1997), *Fractals and Chaos in Geology and Geophysics*, Cambridge Univ. Press, Cambridge, U. K.

D. Akca, Department of Information Technologies, Isik University, 34980 Sile, Istanbul, Turkey.

J. S. Andrade Jr., Departamento de Física, Universidade Federal do Ceará, 60451-970 Fortaleza, Ceará, Brazil.

M. Cavalcanti Tavares, Departamento de Geologia, Universidade Federal do Ceará, Blocos 912/913, 128181 Ceará, Brazil.

M. Doumi, H. J. Herrmann, and H. J. Seybold, Computational Physics, IfB, ETH Zurich, CH-8093 Zurich, Switzerland. (hseybold@ethz.ch)

W. Kinzelbach and P. Molnar, Institute of Environmental Engineering, ETH Zurich CH-8093 Zurich, Switzerland.

T. Shinbrot, Department of Biomedical Engineering, Rutgers University, Piscataway, NJ 08854, USA.